Journal of Power Sources 463 (2020) 228213

Contents lists available at ScienceDirect

Journal of Power Sources

journal homepage: www.elsevier.com/locate/jpowsour

In-situ preparation of Li_xSn-Li_2O–LiF/reduced graphene oxide composite anode material with large capacity and high initial Coulombic efficiency

Rui Xu [a], Yuqi Zhou [b], Liyi Shi [b], Zhuyi Wang [b,**], Yin Zhao [b], Meihong Zhang [b], Shuai Yuan [b,c,*]

[a] Laboratory for Microstructures, Shanghai University, Shanghai, 200444, China
[b] Research Centre of Nanoscience and Nanotechnology, Shanghai University, Shanghai, 200444, China
[c] Emerging Industries Institute, Shanghai University, Jiaxing, Zhejiang, 314006, China

HIGHLIGHTS

- Li_xSn-Li_2O–LiF/RGO composite was obtained by the lithiation of F–SnO_2/RGO.
- Initial Coulombic efficiency of Li_xSn-Li_2O–LiF/RGO composite is as high as 97%.
- The residual capacity is as high as 992 $mAhg^{-1}$ after 100 cycles.

GRAPHICAL ABSTRACT

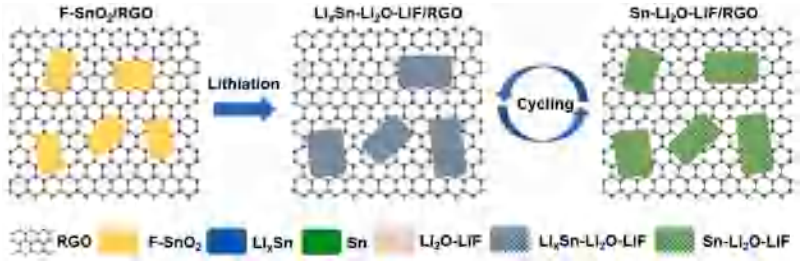

ARTICLE INFO

Keywords:
Anode
Li_xSn-Li_2O–LiF/Reduced graphene oxide
Lithiation
Initial Coulombic efficiency
Cycling stability

ABSTRACT

Anode materials with large capacity have a growing application due to the booming electric vehicle and energy storage market. However, the low initial Coulombic efficiency (ICE) and poor cycle stability hinder their commercial development. Herein, we investigate the effective and convenient method of preparing Li_xSn-Li_2O–LiF/reduced graphene oxide (Li_xSn-Li_2O–LiF/RGO, Li-GFTO) composite anode material with large capacity and high ICE. Firstly, the highly-dispersed fluorine-doped tin oxide and reduced graphene oxide (F–SnO_2/RGO, GFTO) composite is in-situ synthesized by one-pot reflux method. The fluorine-doped SnO_2 nanocrystals are uniformly anchored on graphene sheets. Secondly, the F–SnO_2/RGO was lithiated by reacting with the lithium dissolved in the solution of biphenyl and 1,2-dimethoxyethane to get Li_xSn-Li_2O–LiF/RGO composite. The Li_2O and LiF will be formed and prevent the diffusion and coarsening of Sn and Li_xSn during cycling. Used as the anode material, the ICE of the Li_xSn-Li_2O–LiF/RGO composite is as high as 97%. The composite anode material also shows high cycling stability. The residual capacity is as high as 992 $mAhg^{-1}$ at 0.1 Ag^{-1} after 100 cycles, and the charge capacity retention is 99%. Most of all, the mild preparation condition promotes the mass production and practical application of tin-lithium alloy based composite anode materials.

1. Introduction

With the development of new energy vehicles, the demand for lithium-ion batteries with high energy density and power density is increasing. However, the currently commercial graphite anode has reached its theoretical capacity limit, which prompts people to find new

* Corresponding author. Research Centre of Nanoscience and Nanotechnology, Shanghai University, Shanghai, 200444, China.
** Corresponding author.
E-mail addresses: bamboo2009@shu.edu.cn (Z. Wang), s.yuan@shu.edu.cn (S. Yuan).

https://doi.org/10.1016/j.jpowsour.2020.228213
Received 25 March 2020; Received in revised form 14 April 2020; Accepted 16 April 2020
Available online 24 April 2020

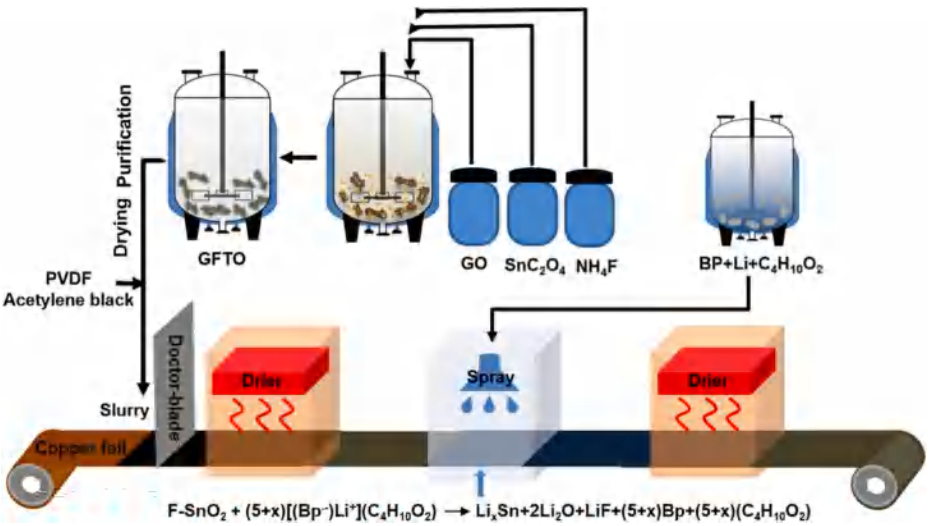

Fig. 1. Illustration of the preparation of Li_xSn-Li_2O–LiF/RGO (Li-GFTO).

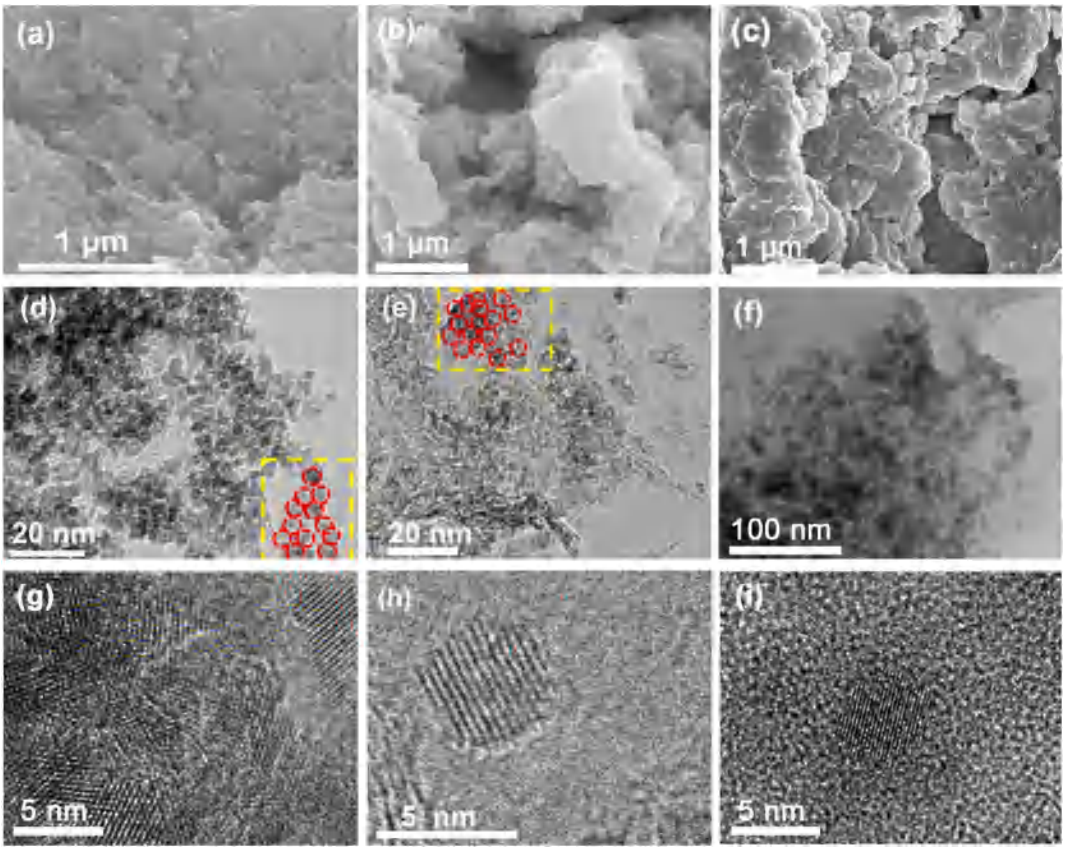

Fig. 2. SEM images of (a) GTO, (b) GFTO and (c) Li-GFTO composites. TEM and HRTEM images of (d, g) GTO, (e, h) GFTO and (f, i) Li-GFTO composites.

anode material. Among various candidates, anode with large capacity like Si-based material and Sn-based material have drawn much attention [1]. Tin oxide (SnO_2) is considered as one of the most promising anode materials due to low cost, environmental friendliness, and high theoretical specific capacity [2]. However, there are two significant obstacles in front of the commercialization of tin dioxide. One is the high irreversible capacity loss in the first cycle, and the other is the severe capacity fading during cycling [3].

The large volume expansion of SnO_2 during charging and discharging leads to electrode pulverization and causes severe capacity decay [4]. Reducing the particles size of SnO_2 can improve the cycle performance by reducing the size of particles could effectively, which can reduce the volume deformation, thus improve the electrochemical performance [5]. Forming anode composites with graphene is also an effective strategy to improve the electrochemical performance [6]. Graphene can not only prevent the agglomeration of the nanoparticles but also alleviate the volume change and improve the electronic conductivity [7]. Meanwhile, dopants like Ti can enhance Li^+ diffusion in the bulk structure [8], F can improve the electronic conductivity and the cycling stability [9,10].

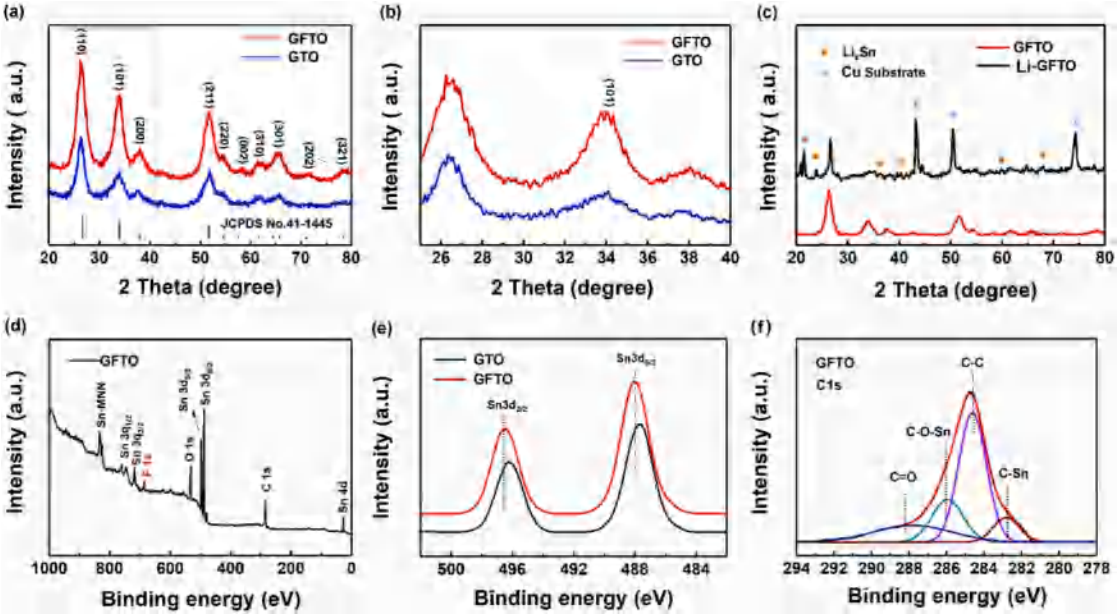

Fig. 3. (a) XRD patterns of the GTO and GFTO composites, (b) extended XRD patterns of the GTO and GFTO composites, (c) XRD patterns of the GFTO and Li-GFTO electrode sheets, (d) XPS curve of the GFTO composite, (e) Sn3d XPS curves of the GTO and GFTO composites, (f) C1s XPS curve of the GFTO composite.

However, the low initial Coulombic efficiency (ICE) of tin oxide-based anode material is still one big obstacle before the application. The formation of solid electrolyte interface (SEI) and the irreversible formation of Li_2O are considered the major reasons for low ICE, which will consume a large amount of liquid electrolyte [11–14]. Coating an inactive protective layer such as carbon or alumina is beneficial to improve the boundary integrity of SnO_2 and stabilize the electrode/electrolyte interface, leading to improved ICE [15–17]. Another route to improve ICE is to add transition metals to stabilize the nanostructure of SnO_2 [18–20]. Hu et al. reported a series of ternary SnO_2-*M*-graphite composites (M = Fe, Mn, Co) prepared by milling SnO_2 with transition metal (M) and graphite powder [18]. The nanometal particles act as a barrier, hindering the migration of Sn from one grain to another, and preventing the coarsening of Sn during the lithiation process. However, the ICE of the samples still can't compare with graphite (about 95%).

Herein, we investigated the effective and convenient method of preparing Li_xSn-Li_2O–LiF/RGO (Li-GFTO) composite anode material with large capacity and high ICE. Firstly, the highly-dispersed F–SnO_2/RGO (GFTO) composite was in-situ synthesized by a one-step reflux method from commercially ammonium fluoride, stannous oxalate, and graphene oxide. Stannous oxalate can reduce graphene oxide directly and form SnO_2 nanocrystals on the graphene sheet. During the growth of SnO_2, fluorine was doped in the lattice simultaneously. Then, the Li metal dissolved in an ether solution containing biphenyl was used to reduce SnO_2 to Li_xSn alloy and produce Li_xSn-Li_2O–LiF/RGO composite, which shows the ICE as high as 97% and excellent cycle stability. The residual capacity is as high as 992 $mAhg^{-1}$ at 0.1 Ag^{-1} after 100 cycles, and the charge capacity retention is 99%. The preparation of Li_xSn-Li_2O–LiF/RGO composite does not need high temperature and high pressure, which is easy to be produced at large-scale.

2. Experiments

2.1. Synthesis of F–SnO_2/RGO (GFTO)

The graphene oxide (GO) was bought from Nanjing XFNANO Materials Tech Company. 1.6 g GO, 12.0 g stannous oxalate was added in 1 L deionized water and stirred for 30 min. Then 4.3 g ammonium fluoride was added in the above solution and stirred for additional 30 min, which offers F element and enables F to be doped into the lattice of SnO_2. At last, the mixture was refluxed at 100 °C for 24 h. The product was filtered and washed by deionized water and ethanol, respectively. After drying at 120 °C for 12h, the F–SnO_2/RGO powder was obtained. The SnO_2/RGO (GTO) was prepared by the same procedure in the absence of ammonium fluoride.

2.2. Preparation of Li_xSn-Li_2O–LiF/RGO (Li-GFTO)

The biphenyl powder was mixed with 1, 2-dimethoxyethane solvent with a molar ratio of 1:9.65 in an argon gas-protected glove box, and stirred for 1 h to completely dissolved. A certain amount of lithium has completely dissolved in the above solution to get the lithiation reagent, wherein the molar ratio of lithium to biphenyl is 1:1 [21].

10.0 mg Polyvinylidene Fluoride (PVDF) and a few drops of N-methyl-2-pyrrolidone (NMP) were added into a 5 mL beaker, stirred until dissolved. The active material (80.0 mg) was uniformly mixed with 10.0 mg acetylene black and stirred for 4h in the above solution to get a slurry. Then, the slurry was coated onto a copper foil and dried at 120 °C for 12 h. The active material loading density is 1.53 mg cm^{-2}. The thickness of the coating layer is 15 μm. Under the protection of argon in glove box, the lithiation reagent was dropped on the anode sheets. After permeation and reaction for 5 min, the samples were dried to get Li_xSn-Li_2O–LiF/RGO (Li-GFTO).

2.3. Characterization

The X-ray diffraction (XRD) patterns were measured on Rigaku D/max-2550 V (Cu Kα radiation, λ = 0.15403 nm) with the scanning range of 10°–85° and the scanning speed of 8° min^{-1}. The monocrystalline silicon wafer has been used to adjust the XRD before the test. X-ray photoelectron spectra (XPS, K-alpha, Thermo Scientific Inc., U.K.) were measured with Mg Kα X-ray radiation, λ = 0.9890 nm. Thermogravimetric analysis (TGA) was carried out on TGA Q800. Transmission electron microscope (TEM) and high-resolution transmission electron microscope (HRTEM) images were obtained on JEOL-2100F equipped with the energy-dispersive X-ray spectroscopy (EDX).

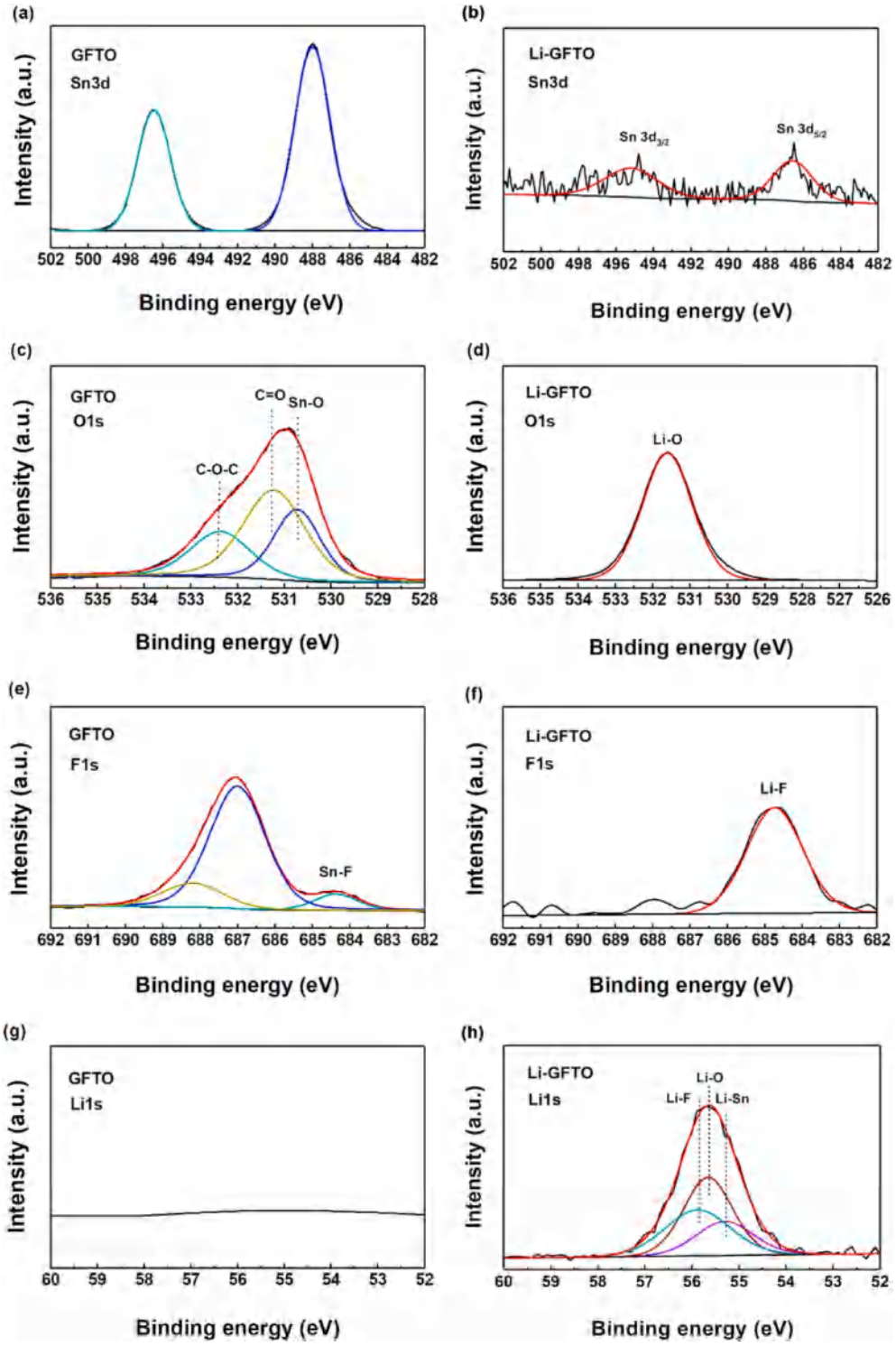

Fig. 4. Sn 3d, O 1s, F 1s and Li 1s XPS curves of the (a), (c), (e), (g) GFTO and (b), (d), (f), (h) Li-GFTO composites.

2.4. Electrochemical measurement

The counter electrode was metallic lithium. The electrolyte was 1 M $LiPF_6$ dissolved in EC/EMC/DMC (volume 1:1:1, Zhangjiagang Guotai-Huarong New Chemical Materials Co., Ltd). The separator was a polypropylene membrane (Celgard 2325). The CR2016 half-cells were assembled in an argon atmosphere glove box (oxygen content $\leq$ 0.5 ppm, water content $\leq$ 0.5 ppm). The cyclic voltammetry (CV) curve was measured by a CHI660E at a scan rate of 0.5 mV s^{-1} in the range of 0.005–3.0 V. Electrochemical impedance spectroscopy (EIS) was measured on a Metrohm Autolab PGSTAT302 N electrochemical workstation. A LAND-CT 2001A test system was used to measure the cycle and rate performance between 0.01 and 3.0 V (T = 25 °C, humidity $\leq$ 15%).

3. Results and discussion

Fig. 1 illustrates the process of preparing Li_xSn-Li_2O–LiF/RGO (Li-

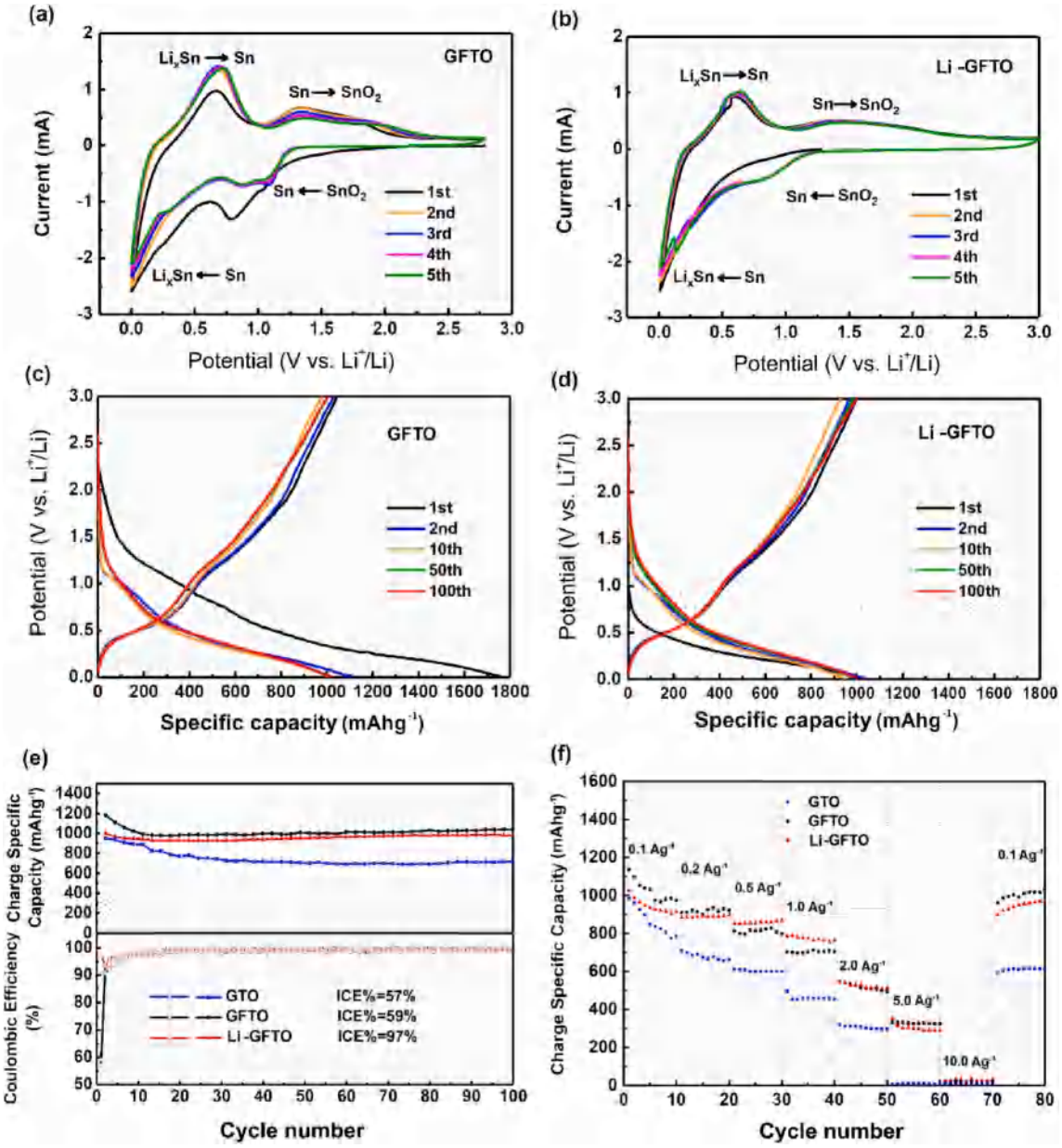

Fig. 5. CV curves of (a) GFTO and (b) Li-GFTO composites; Galvanostatic charge and discharge profiles of (c) GFTO and (d) Li-GFTO composites; (e) Cycling performance of GTO, GFTO, and Li-GFTO electrodes at 0.1 A g^{-1},(f) Rate capability of GTO, GFTO, and Li-GFTO electrodes.

GFTO) composites. Firstly, the F–SnO_2/RGO (GFTO) composite is one-pot synthesized from the commercial raw materials stannous oxalate, ammonium fluoride and graphene oxide by the reflux method at atmospheric pressure. Sn^{2+} ions were oxidized by graphene oxide to form SnO_2 and reduced graphene oxide. Simultaneously, the fluorine was doped into the lattice of SnO_2. The reaction does not need high temperature and high pressure, which is simple and easy to realize mass production. Secondly, the slurry containing GFTO, PVDF and acetylene black was coated on copper foil. Then, the anode was lithiated by lithium dissolved in biphenyl. After drying to remove solvent, the Li_xSn-Li_2O–LiF/RGO composites was produced. According to the process, it has high potential to realize the large-scale production.

3.1. Morphology analysis

Fig. 2a–c shows the SEM images of GTO, GFTO and Li-GFTO composites. All of them have a similar layered sponge structure, indicating the lithiation did not destroy such structure. The combination of F–SnO_2 and graphene oxide (GO) sheets makes F–SnO_2 nanoparticles in GFTO dispersed more uniform than SnO_2 nanoparticles in GTO (Fig. 2d and e). F–SnO_2 nanoparticles are not agglomerated and not scattered outside the graphene sheets, indicating that F–SnO_2 nanoparticles can uniformly anchor on graphene sheets to form a uniform structure by one-pot reflux method [22]. Meanwhile, F element uniformly dispersed in GFTO composite, confirmed by the element distribution (Fig. S1). As shown in Fig. 2d–e, the average particle size of the SnO_2 and F–SnO_2 nanoparticles is less than 10 nm. It could be observed that the lattice spacing of 0.26 and 0.33 nm corresponds to the (101) and (110) crystal planes of SnO_2 from Fig. 2g and h [10]. In addition, the content of SnO_2 in GFTO is 79.8% from TG result (Fig. S2), which is beneficial to the large capacity of the material. After lithiation, the nanoparticles apparently become larger because of the insertion of lithium, but there is still no obvious agglomeration, which may be due to the formation of Li_2O and LiF (Fig. 2f). The lattice spacing of 0.23 nm should correspond to the (331) crystal plane of Li_7Sn_2 (Fig. 2i).

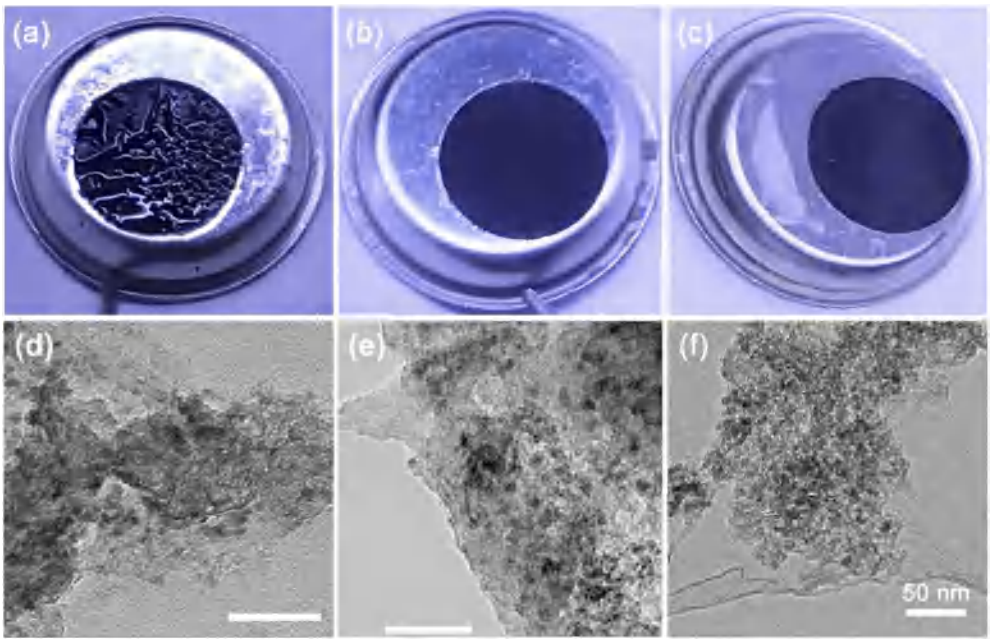

Fig. 6. Pictures of the (a) GTO, (b) GFTO and (c) Li-GFTO electrodes after the 100th cycle at 0.1 A g^{-1} and the corresponding TEM images of (d) GTO, (e) GFTO and (f) Li-GFTO electrodes after the 100th cycle at 0.1 A g^{-1}.

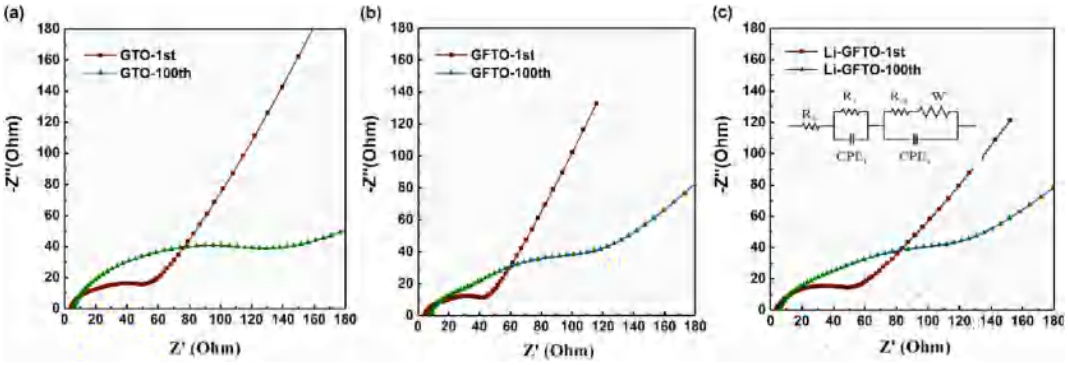

Fig. 7. EIS of (a) GTO, (b) GFTO and (c) Li-GFTO electrodes measured after 1st cycle and 100th cycle and the equivalent circuit model inset.

Table 1
The fitted and calculated results of the kinetic parameters of GTO, GFTO and Li-GFTO electrodes after 1st cycle and 100th cycle.

Sample	GTO		GFTO		Li-GFTO	
	R_f (Ω)	R_{ct} (Ω)	R_f (Ω)	R_{ct} (Ω)	R_f (Ω)	R_{ct} (Ω)
1st cycle	12.9	27.9	11.4	21.7	12.4	26.8
100th cycle	29.8	113	18.8	93	20.7	95.6

3.2. Component analysis

Fig. 3a shows a typical X-ray diffraction pattern of GTO and GFTO composites. All the peaks of GTO and GFTO composites can be identified as a tetragonal rutile-like SnO_2 (JCPDS No.41–1445). There is no appearance of a hetero peak, indicating that Sn^{2+} is completely oxidized to SnO_2, then SnO_2 heterogeneously nucleate and grow. From the partial enlargement of XRD (Fig. 3b), the diffraction peaks of GFTO slightly shifted to a smaller angle than GTO, indicating that F was doped into the lattice of SnO_2 instead of merely attaching to the crystal surface [23]. The XRD diagram of lithiated sample Li_xSn-Li_2O–LiF/RGO (Li-GFTO) (Fig. 3c) shows that Li_xSn is mainly attributed to Li_5Sn_2 (JCPDS 29–0839) and Li_7Sn_2 (JCPDS 29–0837).

From the full XPS diagram of GFTO, the peak of doping F could be observed clearly (Fig. 3d). The diagram (Fig. 3e) of Sn 3d shows that the peaks at 488.0 eV and 496.4 eV corresponds to the peaks of SnO_2. The binding energy difference between $Sn3d_{5/2}$ and $Sn3d_{3/2}$ is 8.4 eV, which is consistent with the energy splitting of SnO_2 [20]. Compared with GTO, the Sn 3d binding energy of GFTO shifts to higher levels. It may be due to the large electronegativity of fluorine, decreasing the electron density in the 3d orbital of Sn [23]. The results also confirm that fluorine was doped in the lattice of SnO_2. The C 1s peaks of GFTO (Fig. 3f) are de-convoluted into four peaks, and the peaks at 282.8 and 285.9 eV are attributed to the oxygen-containing functional groups C–O left on the graphene sheets and C–Sn bond formed by reflux method [17]. According to the XPS results, F–SnO_2 nanoparticles may combine with graphene by C–O–Sn and Sn–C bonds [24,25]. The strong interaction between F–SnO_2 nanoparticles and graphene is beneficial for the uniform growth of SnO_2 and the structural stability of GFTO [26,27].

To better understand the process of lithiation, the XPS spectra of Sn 3d, F 1s, O 1s, Li 1s branches of samples F–SnO_2/RGO (GFTO), and Li_xSn-Li_2O–LiF/RGO (Li-GFTO) were analyzed and compared in Fig. 4. Fig. 4a shows two typical peaks at 488.0 eV and 496.4 eV, belonging to SnO_2 before lithiation. Two weak peaks at 486.6 and 495.1 eV appears after lithiation in Sn 3d spectrum (Fig. 4b), which should be attributed to

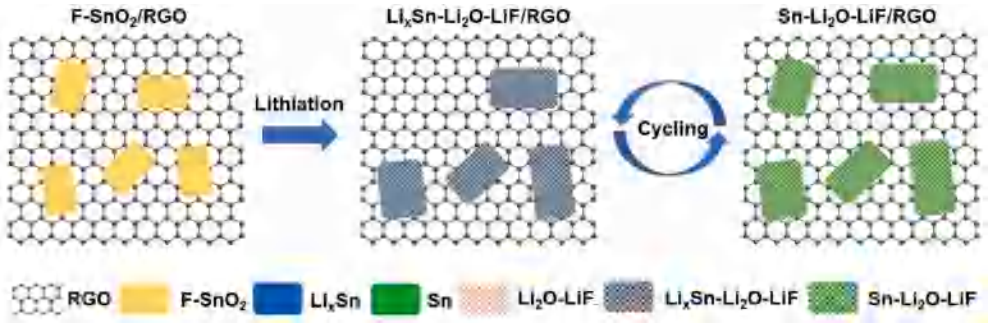

Fig. 8. Illustration of the cycling stability of Li_xSn-Li_2O–LiF/RGO (Li-GFTO).

Li_xSn [28]. In the O 1s spectra, three peaks located at 530.7, 531.3 and 532.5 eV belonging to Sn–O, C═O and C–O–C bonds (Fig. 4c) were replace by the peak at 531.6 eV after lithiation, which should be attributed to Li_2O (Fig. 4d) [29]. Fig. 4e shows F 1s peaks at 688.3, 686.9 and 684.4 eV ascribing to F in binder PVDF and Sn–F bond, respectively [30,31]. After lithiation, the peak at 684.7 eV is attributed to the formation of Li–F (Fig. 4f) [32]. Similarly, there are obvious peaks of Li–Sn, Li–O and Li–F at 55.3, 55.6 and 55.9 eV after lithiation in the Li 1s spectrum (Fig. 4h) [33,34]. Thus, the reduction of SnO_2 and formation of Li_xSn after lithiation can be confirmed through the comparison of XPS spectra, which agrees with the XRD analysis results well.

3.3. Electrochemical performance

Based on the above analysis, it can be confirmed that the fluorine is doped into the lattice of SnO_2 and F–SnO_2 nanoparticles are uniformly anchored on the graphene sheets. The process of lithiation can reduce SnO_2 to Li_xSn. To investigate the potential of application in lithium ion battery as anode materials, their electrochemical properties are measured and discussed.

Fig. 5a and b exhibit the CV curves of the first five cycles of GFTO and Li-GFTO composites. For GFTO, the reduction peak at around 1.0 V represents a reduction reaction from SnO_2 to Sn, accompanying the formation of Li_2O and LF, as Eq. (1) [35]. The peak around 0.7 V in the first cathodic scan indicates that the material reacted with the electrolyte and formed a solid electrolyte interface (SEI). However, these peaks do not appear in the first cycle of the Li-GFTO electrode due to the formation of Li_xSn alloy, which is consistent with the characterization of XRD and XPS. The reduction peak appearing around 0.1 V reflects the formation of Li_xSn alloy, and the insertion of Li^+ into graphene, as Eq. (2) and Eq. (3) [35]. GFTO and Li-GFTO electrodes both have a good curve coincidence, reflecting that these composites have good electrochemical stability. Fig. 5c and d displays the galvanostatic charge-discharge profiles at the 1st, 2nd, 10th, 50th, and 100th cycles of GFTO and Li-GFTO composites. The low initial Coulombic efficiency (ICE) of GFTO is mainly owing to the formation of SEI and lithium oxide [35,36]. The initial voltage and the initial capacity of Li-GFTO are significantly reduced after lithiation. The voltage platform representing the reduction process of SnO_2 around 1.0 V disappeared, which means the reaction SnO_2 reduced to Sn is disappeared. Consequently, the formation of Li_2O is avoided and as a result more Li^+ is prevented from consumption, leading to an improved ICE. The behaviors during charge and discharge agree well with CV curves, confirming that the lithiation can improve the ICE without scarifying the cycle stability.

$$SnO_{2-x}F_x + (4-x)Li^+ + (4-x)e^- \rightarrow Sn + (2-x)Li_2O + xLiF \quad (1)$$

$$Sn + xLi^+ + xe^- \leftrightarrow Li_xSn \quad (2)$$

$$C(Graphene) + xLi^+ + xe^- \leftrightarrow Li_xC \quad (3)$$

The cycling curves and Coulombic efficiency curves are shown in Fig. 5e. The ICE values of GTO, GFTO and Li-GFTO are 57%, 59%, and 97%, respectively. The initial capacities of GTO, GFTO, and Li-GFTO are 950, 1180 mAh g^{-1}, and 999 mAh^{-1}, and the charge capacity retention are 80%, 89%, and 99% after 100 cycles, respectively. GFTO and Li-GFTO electrodes have the higher reversible capacity and cycle stability than GTO electrodes. Meanwhile, they also exhibited good rate performance (Fig. 5f and Table S1). At the current of 1.0 A g^{-1}, the charge capacity of GFTO and Li-GFTO electrodes can maintain 73% and 82% of the capacity, while the GTO can only maintain 54%. It should be ascribed to the fluorine doping which improved the electronic conductivity and facilitates the rapid transmission of electrons [23]. In addition, the GFTO and Li-GFTO electrodes can restore the high reversible charge capacity after rapid charge and discharge. As a result, the lithiated sample Li_xSn-Li_2O–LiF/RGO (Li-GFTO) shows obviously improved initial Coulomb efficiency, cycle stability and rate performance.

To further investigate the structural stability, the morphology and structure of the electrode materials after 100 cycles were detected by TEM. From the pictures of electrodes after 100 cycles (Fig. 6a–c), there is no wrinkle on the surface of GFTO and Li-GFTO electrodes macroscopically compared with GTO. Correspondingly, there is an obvious agglomeration of particles on GTO anode (Fig. 6d). In contrast, the dispersion of particles on graphene in GFTO and Li-GFTO composites is still uniform after cycling (Fig. 6e and f) (Fig. S3) [22], which confirms that the formation of LiF after lithiation can prevent the diffusion of Sn/Li_xSn across one grain to the other grains, which effectively suppressed coarsening and improved the conversion rate of the reaction between Li_2O and Sn/Li_xSn, which is beneficial to the reaction reversibility during cycling. Therefore, GFTO and Li-GFTO electrodes have better cyclic stability.

As shown in Fig. 7, the electrochemical impedance spectroscopy of GTO, GFTO and Li-GFTO electrodes are measured in the frequency range from 0.1 Hz to 1 MHz. The Nyquist plots are fitted by an equivalent circuit (inset in Fig. 7) and the kinetic parameters are summarized in Table 1. R_f and R_{ct} represent the contact resistant of SEI film and charge transfer resistant, respectively. R_f and R_{ct} of GTO electrode are slightly larger than those of GFTO and Li-GFTO electrode after the 1st cycle, indicating that the doping of F can increase electronic conductivity. After 100th cycle, R_f and R_{ct} of GTO electrode are obviously larger than those of GFTO and Li-GFTO electrode, which may be related to the structural stability of electrodes.

4. Conclusion

In summary, a fluorine-doped tin oxide and reduced graphene oxide (F–SnO_2/RGO, GFTO) composite was synthesized by a one-pot reflux method. Fluorine-doped SnO_2 can uniformly grow on the graphene sheet to form a stable structure. The Li_xSn-Li_2O–LiF/RGO (Li-GFTO) was produced from GFTO by lithiation to reduce SnO_2 to Li_xSn. The formation of LiF can effectively prevent the agglomeration of Sn and Li_xSn, which is beneficial to the reaction reversibility during cycling (Fig. 8). The ICE of Li_xSn-Li_2O–LiF/RGO is as high as 97%. The residual capacity

is as high as 992 mAh g^{-1} at 0.1 A g^{-1} after 100 cycles, and the charge capacity retention is 99%. Significantly, the mild preparation condition promotes the mass production and practical application of tin-based anode with large capacity.

Declaration of competing interest

The authors declare that they have no known competing financial interests or personal relationships that could have appeared to influence the work reported in this paper.

CRediT authorship contribution statement

Rui Xu: Visualization, Writing - review & editing. **Yuqi Zhou:** Investigation, Writing - original draft. **Liyi Shi:** Resources. **Zhuyi Wang:** Methodology, Supervision. **Yin Zhao:** Formal analysis. **Meihong Zhang:** Formal analysis. **Shuai Yuan:** Conceptualization, Funding acquisition, Supervision.

Acknowledgements

The authors acknowledge the National Natural Science Foundation of China (51711530162, 21503131) and Science and Technology Commission of Shanghai Municipality (15DZ1170100, 19640770300) for financial support.

Appendix A. Supplementary data

Supplementary data related to this article can be found at https://doi.org/10.1016/j.jpowsour.2020.228213.

References

[1] L. Zhu, Y. Chen, C. Wu, R. Chu, J. Zhang, H. Jiang, Y. Zeng, Y. Zhang, H. Guo, Double-carbon protected silicon anode for high performance lithium-ion batteries, J. Alloys Compd. 812 (2020) 151848.
[2] J.S. Chen, X.W. Lou, SnO_2-based nanomaterials: synthesis and application in lithium-ion batteries, Small 9 (2013) 1877–1893.
[3] J. Leng, Z.X. Wang, X.H. Li, H.J. Guo, G.C. Yan, Q.Y. Hu, W.J. Peng, J.X. Wang, A novel dried plum-like yolk-shell architecture of tin oxide nanodots embedded into carbon matrix: ultra-fast assembly and superior lithium storage property, Mater. Chem. A. 7 (2019) 5803–5810.
[4] H. Kim, G.O. Park, Y. Kim, S. Muhammad, J. Yoo, M. Balasubramanian, Y.H. Cho, M.G. Kim, B. Lee, K. Kang, H. Kim, J.M. Kim, W.S. Yoon, New insight into the reaction mechanism for exceptional capacity of ordered mesoporous SnO_2 electrodes via synchrotron-based X-ray analysis, Chem. Mater. 26 (2014) 6361–6370.
[5] X.W. Lou, J.S. Chen, P. Chen, L.A. Archer, One-Pot Synthesis of carbon-coated SnO_2 nanocolloids with improved reversible lithium storage properties, Chem. Mater. 21 (2009) 2868–2874.
[6] H. Chen, K. Shen, X. Hou, G. Zhang, S. Wang, F. Chen, L. Fu, H. Qin, Y. Xia, G. Zhou, Si-based anode with hierarchical protective function and hollow ring-like carbon matrix for high performance lithium ion batteries, Appl. Surf. Sci. 470 (2019) 496–506.
[7] Y.Q. Sun, Q.O. Wu, G.Q. Shi, Graphene based new energy materials, Energy Environ. Sci. 4 (2011) 1113–1132.
[8] L.W. Liang, X. Sun, J.Y. Zhang, L.R. Hou, J.F. Sun, Y. Liu, S.G. Wang, C.Z. Yuan, In situ synthesis of hierarchical core double-shell Ti-Doped $LiMnPO_4$@$NaTi_2(PO_4)_3$@C/3D Graphene cathode with high-rate capability and long cycle life for lithium-ion batteries, Adv. Energy Mater. (2019) 1802847.
[9] M. Kim, K.H. Kim, M.J. Kim, J.G. Kim, Y.S. Lee, The synergistic effect of fluorination and embedded SnO_2 on the NO gas sensing of expanded graphite, Mater. Res. Bull. 116 (2019) 44–49.
[10] S. Wang, L. Shi, G. Chen, C. Ba, Z. Wang, J. Zhu, Y. Zhao, M. Zhang, S. Yuan, In situ synthesis of tungsten-doped SnO_2 and graphene nanocomposites for high-performance anode materials of lithium-ion batteries, ACS Appl. Mater. Interfaces 9 (2017) 17164–17172.
[11] H.X. Zhang, C. Feng, Y.C. Zhai, K.L. Jiang, Q.Q. Li, S.S. Fan, Cross-stacked carbon nanotube sheets uniformly loaded with SnO_2 nanoparticles: a novel binder-free and high-capacity anode material for lithium-ion batteries, Adv. Mater. 21 (2009) 2299–2304.
[12] X. Wang, X.Q. Cao, L. Bourgeois, H. Guan, S.M. Chen, Y.T. Zhong, D.M. Tang, H. Q. Li, T.Y. Zhai, L. Li, Y. Bando, D. Golberg, N-doped graphene-SnO_2 sandwich paper for high-performance lithium-ion batteries, Adv. Funct. Mater. 22 (2012) 2682–2690.
[13] X.S. Zhou, L.J. Wan, Y.G. Guo, Binding SnO_2 nanocrystals in nitrogen-doped graphene sheets as anode materials for lithium-ion batteries, Adv. Mater. 25 (2013) 2152–2157.
[14] L.W. Liang, X. Sun, J.Y. Zhang, J.F. Sun, L.R. Hou, Y. Liu, C.Z. Yuan, Sur-/interfacial regulation in all-solid-state rechargeable Li-ion batteries based on inorganic solid-state electrolytes: advances and perspectives, Mater. Horiz. 6 (2019) 871–910.
[15] W.H. Xie, L.L. Gu, F.Y. Xia, B.L. Liu, X.Y. Hou, Q. Wang, D.Q. Liu, D.Y. He, Fabrication of voids-involved SnO_2@C nanofibers electrodes with highly reversible Sn/SnO_2 conversion and much enhanced coulombic efficiency for lithium-ion batteries, J. Power Sources 327 (2016) 21–28.
[16] Y.X. Wan, L.J. Wang, Y.J. Chen, X.Q. Xu, Y. Wang, C. Teng, D.S. Zhou, Z.J. Chen, A high-performance tin dioxide@carbon anode with a super high initial coulombic efficiency via a primary cell prelithiation process, J. Alloys Compd. 740 (2018) 830–835.
[17] H.P. Zhang, Z.W. Chen, R.Z. Hu, J. Liu, J. Cui, W.J. Zhou, C.H. Yang, Enabling a highly reversible conversion reaction in a lithiated nano-SnO_2 film coated with Al_2O_3 by atomic layer deposition, J. Mater. Chem. A. 6 (2018) 4374–4385.
[18] R.Z. Hu, Y.P. Ouyang, T. Liang, H. Wang, J. Liu, J. Chen, C.H. Yang, L.C. Yang, M. Zhu, Stabilizing the nanostructure of SnO_2 anodes by transition metals: a route to achieve high initial coulombic efficiency and stable capacities for lithium storage, Adv. Mater. 29 (2017) 1605006.
[19] P. Deng, J. Yang, S.Y. Li, T.E. Fan, H.H. Wu, Y. Mou, H. Huang, Q.B. Zhang, D. L. Peng, B.H. Qu, High initial reversible capacity and long life of ternary SnO_2-Co-carbon nanocomposite anodes for lithium-ion batteries, Nano-Micro Lett. 11 (2019) 18.
[20] H.P. Xu, S. Yuan, Z.Y. Wang, Y. Zhao, J.H. Fang, L.Y. Shi, Graphene anchored with ZrO_2 nanoparticles as anodes of lithium ion batteries with enhanced electrochemical performance, RSC Adv. 4 (2014) 8472–8480.
[21] G. Chu, B.N. Liu, F. Luo, W.J. Li, H. Lu, L.Q. Chen, H. Li, Conductivity and applications of Li-biphenyl-1,2-dimethoxyethane solution for lithium ion batteries, Chin. Phys. B 26 (2017), 078201.
[22] H.P. Xu, L.Y. Shi, Z.Y. Wang, J. Liu, J.F. Zhu, Y. Zhao, M.H. Zhang, S. Yuan, Fluorine-doped tin oxide nanocrystal/reduced graphene oxide composites as lithium ion battery anode material with high capacity and cycling stability, ACS Appl. Mater. Interfaces 7 (2015) 27486–27493.
[23] J.H. Sun, L.H. Xiao, S.D. Jiang, G.X. Li, Y. Huang, J.X. Geng, Fluorine-doped SnO_2@graphene porous composite for high capacity lithium-ion batteries, Chem. Mater. 27 (2015) 4594–4603.
[24] C.H. Xu, B.H. Xu, Y. Gu, Z.G. Xiong, J. Sun, X.S. Zhao, Graphene-based electrodes for electrochemical energy storage, Energy Environ. Sci. 6 (2013) 1388–1414.
[25] S. Park, J.H. An, I.W. Jung, R.D. Piner, S.J. An, X.S. Li, A. Velamakanni, R.S. Ruoff, Colloidal suspensions of highly reduced graphene oxide in a wide variety of organic solvents, Nano Lett. 9 (2009) 1593–1597.
[26] M. Zhang, D. Lei, Z.F. Du, X.M. Yin, L.B. Chen, Q.H. Li, Y.G. Wang, T.H. Wang, Fast synthesis of SnO_2/graphene composites by reducing graphene oxide with stannous ions, J. Mater. Chem. 21 (2011) 1673–1676.
[27] Y.Z. Jiang, Y. Xu, T.Z. Yuan, M. Yan, Phase-tailored synthesis of tin oxide-graphene nanocomposites for anodes and their enhanced lithium-ion battery performance, Mater. Lett. 91 (2013) 16–19.
[28] C.D. Gu, Y.J. Mai, J.P. Zhou, Y.H. You, J.P. Tu, Non-aqueous electrodeposition of porous tin-based film as an anode for lithium-ion battery, J. Power Sources 214 (2012) 200–207.
[29] I. Epelboin, M. Froment, M. Garreau, J. Thevenin, D. Warin, Behavior of secondary lithium and aluminum-lithium electrodes in propylene carbonate, J. Electrochem. Soc. 127 (1980) 2100–2104.
[30] D. Shuttleworth, Preparation of metal-polymer dispersions by plasma techniques. An ESCA investigation, J. Phys. Chem. 84 (1980) 1629–1634.
[31] M. Davies, High Resolution XPS of Organic Polymers: the Scienta ESCA300 Database, in: G. Beamson, D. Briggs (Eds.), Surf. Interface Anal. vol. 20, John Wiley, Chichester, UK, 1992, p. 267, 1993.
[32] G.E. Murch, R.J. Thorn, Relation between orbital binding energies and ionicities in alkali and alkaline earth flourides, J. Phys. Chem. Solid. 41 (1980) 785–791.
[33] M.L. Casella, G.J. Siri, G.F. Santori, O.A. Ferretti, M.M. Ramirez-Corredores, Surface characterization of Li-modified platinum/tin catalysts for isobutane dehydrogenation, Langmuir 16 (2000) 5639–5643.
[34] K.K.D. Ehinon, S. Naille, R. Dedryvere, P.E. Lippens, J.C. Jumas, D. Gonbeau, Ni_3Sn_4 electrodes for Li-ion batteries: Li-Sn alloying process and electrode/electrolyte interface phenomena, Chem. Mater. 20 (2008) 5388–5398.
[35] Y. Chen, B.H. Song, R.M. Chen, L. Lu, J.M. Xue, A study of the superior electrochemical performance of 3 nm SnO_2 nanoparticles supported by graphene, Mater. Chem. A. 2 (2014) 5688–5695.
[36] S. Xin, Y.G. Guo, L.J. Wan, Nanocarbon networks for advanced rechargeable lithium batteries, Acc. Chem. Res. 45 (2012) 1759–1769.